

MULTI-WELL SAND PRODUCTION PREDICTION STUDY TO SUPPORT FIELD DEVELOPMENT PLAN, LOWER ACACUS FORMATION, AREA 47, GHADAMIS BASIN

M. S. Gheddida*, C. Sorge**, M. El Mabrouk*, A. A. Fituri* and A. V. Der Berken**

Abstract: This work presents the synthesis of an extensive study on sand production prediction conducted on six structures in block 2, Lower Acacus Formation, Area-47 in Ghadamis Basin, Libya. These structures, upon declaring their commerciality, were identified for North Hamada Field Development. Thirteen wells (exploratory and appraisals), have been drilled and tested in these structures. Some of these wells have exhibited sand production phenomena during their initial production tests. A sand production prediction study was performed to investigate and quantify the magnitude of the problem, suggesting proper sand control remedy and optimum completion parameters for cased and open hole scenarios.

Geomechanical Modeling and Wellbore Stability (WBS) Analysis have been performed simultaneously for each well, to assess mechanical properties and stresses that have been used for sanding analysis. A petrophysical and rock physics analysis of log data from all wells allowed to integrate available measurements by means of multi-well workflows utilizing, 1D-geomechanic model, rock physics and completion modules. All analyses confirmed the occurrence of sanding in some critical sections at different reservoir pressure depletion regimes. Predicted sanding tendency on existing wells, was in good agreement, with observations made from DST's.

These results have been used to start planning for the upcoming operation phase. They also constitute the base for the development of an integrated 3D geomechanic reservoir model enabling large scale analysis of the regional sand production phenomena.

Keywords: Area-47, Mechanical earth modeling, Sand production prediction.

INTRODUCTION

Field Location and History

North Hamada Field is located in the North Ghadamis Basin, Libya, approximately 220km South West of Tripoli. The field was discovered in 2005 by Verenex and Medco International Ventures Limited (MIVL) which was operating in Area-47 under Exploration and Production Sharing Agreement (EPSA). The field is divided into 4 blocks with several structures (Oil & Gas) had been proved through exploration wells. The productive structures are mostly located in Block-2 and Block-4 as shown in (Fig.1).

The discovery well is A1-47/02 which penetrated the reservoir main producing sandstone of the Lower Acacus Formation (Silurian). Until very recently, the majority of the exploration focus

has been in Block 2 where thirteen (13) wells have been drilled in order to delineate and test the Acacus Formation. Six (6) proven structures designated AL, B, C, D, F and J already have commercial status through final appraisal report document. Those structures have been engaged in field development plan (FDP) and granted to deliver hydrocarbon from several multilayer from bottom to top (Sand 1 to Sand 5). Some of these drilled wells produce sand during the initial DST performed during the exploration phase.

Objectives

The multi-well sand production study was conducted with the intent to determine if the known sand production during the drill steam tests (DST) can be predicted at the reservoir levels and can be produced to the surface facilities. Therefore, the main identified objectives of this study are:

- 1) Integrate and analyze the existing relevant logs and other field data.

*Nafusah Oil Operation B.V., Tripoli, Libya.

**Schlumberger, Paris, France.

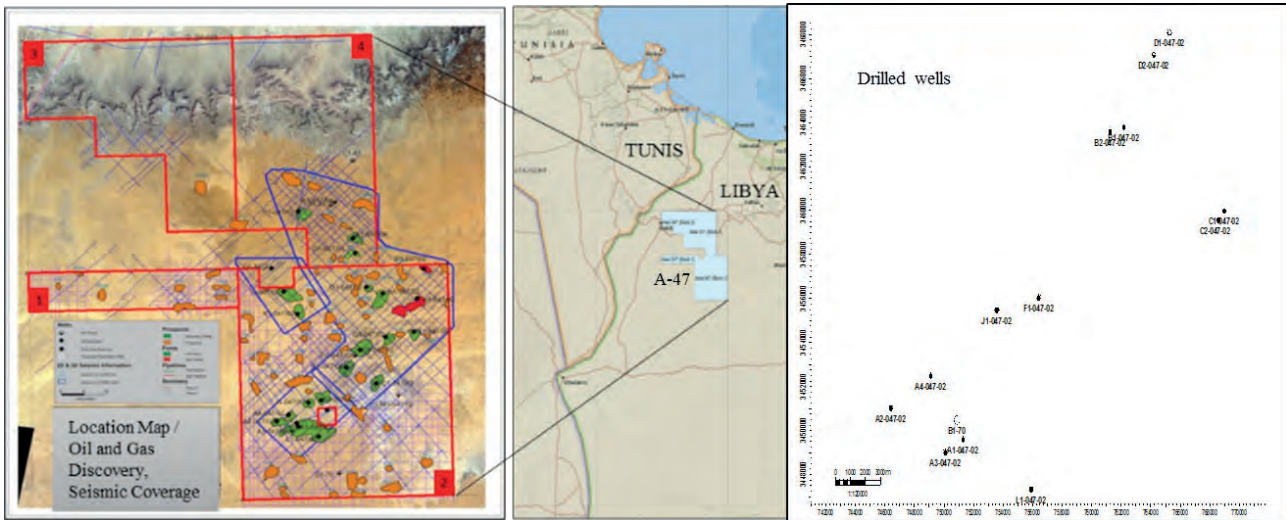


Fig. 1. Location map of the area A 47 and the drilled wells in block 2.

- 2) Perform 1D Mechanical Earth Models (MEM) for the existing 13 wells.
- 3) Perform laboratory tests on selective core samples.
- 4) Refine and calibrate the Mechanical Earth Models, (MEM) using the selected core tests results, existing caliper, drilling data and borehole images.
- 5) Develop continuous critical drawdown profile for the entire reservoir for different depletion steps and for various completion scenarios.
- 6) Perform uncertainty analysis on critical drawdown profile and advice on key inputs to reduce the uncertainty.

RESERVOIR LITHOLOGY

The Lower Acacus Formation consists of multilayers of sandstone, shale and siltstone. Units were interpreted to be for the most part with thick beds of sandstone which also display evidence of textural heterogeneity. Siltstone was interpreted to be a gradation of both sandstone and shale units.

The stratigraphic and structure correlation are constructed through all wells in area 47 Block 2 covering AL, J, F and B, C, D structures. Although the separation between structures is big, the sand continuity from well to well can be clearly observed. The stratigraphic sequence is commonly characterized by cyclic progradational parasequence, and good correlation from well to well in the lower zones as supported by seismic.

It gradually becomes more complicated in

upper zones from Sand 4 up due to deeper marine influence as indicated by more shale interval intercalation. The base reservoir is defined to exclude non-reservoir zones below the pay zones.

To better characterize the reservoir, the key reservoir zones (Sand 1, Sand 2, Sand 3, Sand 4 and Sand 5) are subdivided into several reservoir subzones as shown in stratigraphic cross section (Fig. 2). Each region is indicated by consistent shale or porosity breaks from well to well and tends to have its own fluid contact. The following is the subdivision of the reservoir zones that represents the structures of the study area A, J, F, B and D that are used for static reservoir modeling.

SAND PRODUCTION PREDICTION

Data Audit and Rock Physics

The main results and initial phase of the study is to audit the available data and examine the rock physics. The relevant data typically includes survey, drilling, logs, laboratory and in-situ test data, geological information.

The available logs show good coverage. A minimum log suite allowing a satisfactory geomechanical modeling. All 13 wells were included and used in the study (Fig. 3). eleven wells have compressional sonic (DTCO) whereas shear sonic (DTSM) is available only on four wells.

Editing were performed to fill the gaps and correct the bad obvious reading. Synthetic logs used where measured data show some reading problems or not existing (Fig. 4). For the overburden, synthetic density

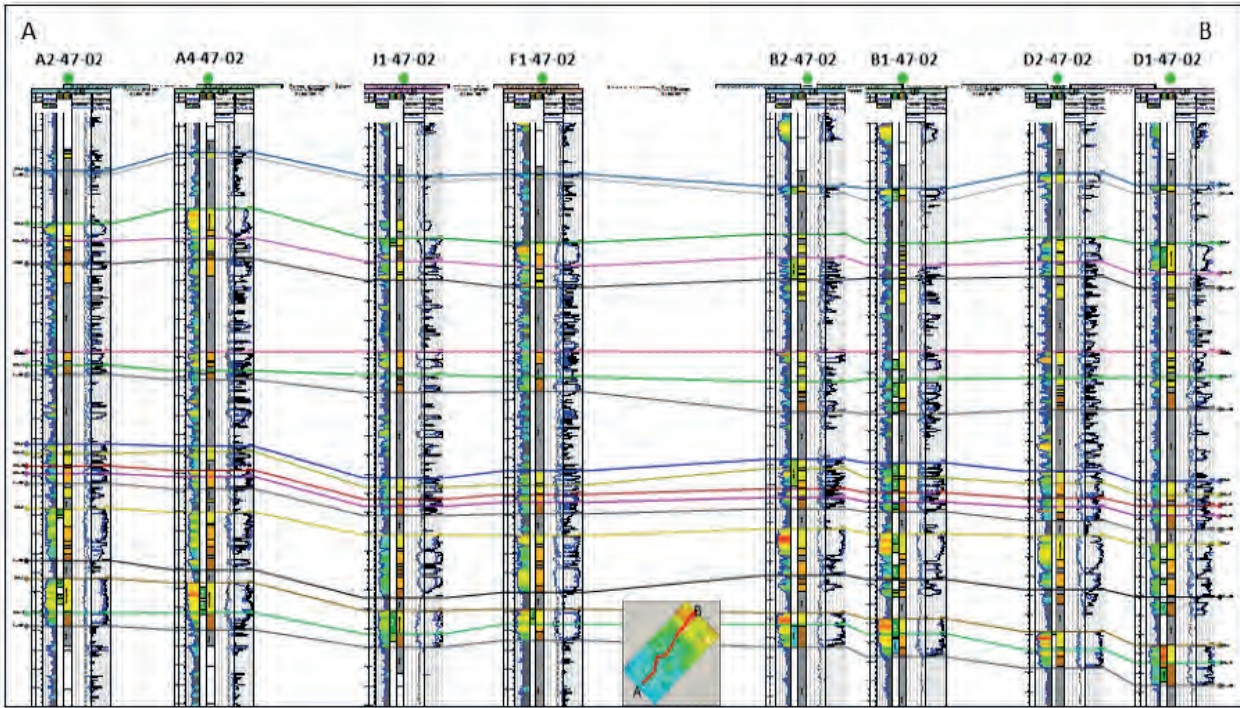


Fig. 2. Lithostratigraphic correlation through the reservoir multilayer.

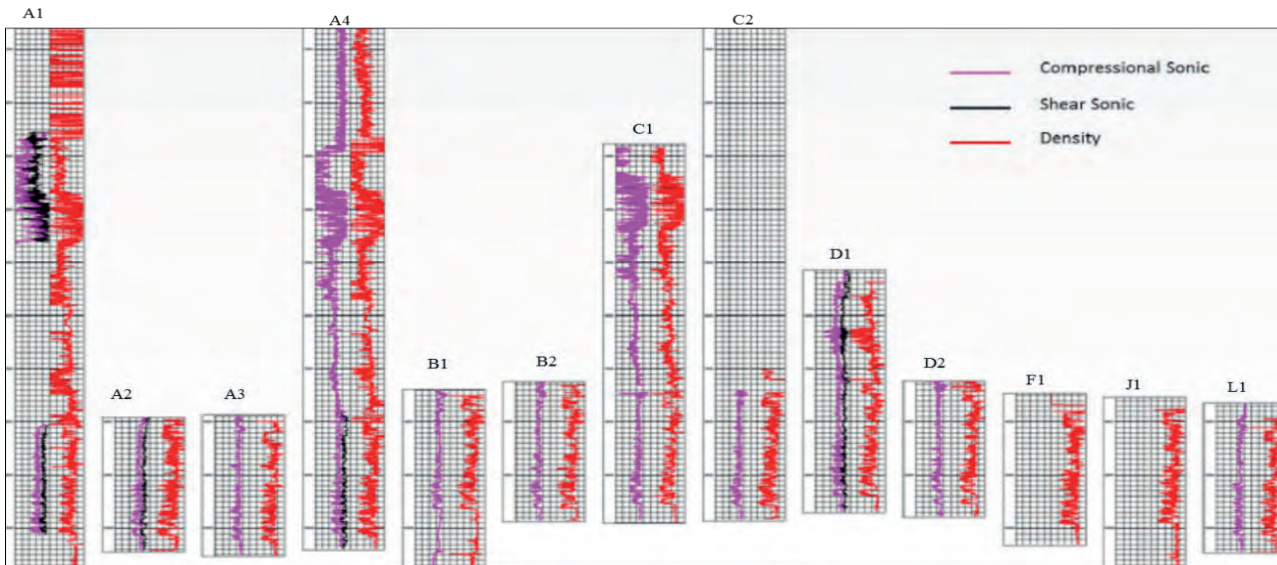


Fig. 3. Shows the provided compressional and share sonic slowness and density in terms of log view. Measured data.

logs have been generated using Gardner relation from literatures for sand and shale.

$$RHOB_{sand} = 1.66 Vp^{0.261}$$

$$RHOB_{shale} = 1.75 Vp^{0.26}$$

The log view gives a good sketch of log coverage (density) and missed data (share). The cross plots help to test the compatibility of the data from the set of wells and QC the available data which proved to be relatively good. The editing start with compressional sonic. A synthetic curve is generated using Neural

Network (NN) technique with logs like measured depth, gamma ray, deep resistivity and neutron porosity as input. The modeled logs are compared to the measured one. Where the condition of the measured log is bad, usually in bad borehole section or not existent, the synthetic log is used in replacement.

The edited compressional sonic is then used as input to edit shear sonic and density log. For overburden (logs are noisier and absence of logs like deep resistivity and neutron porosity) synthetic

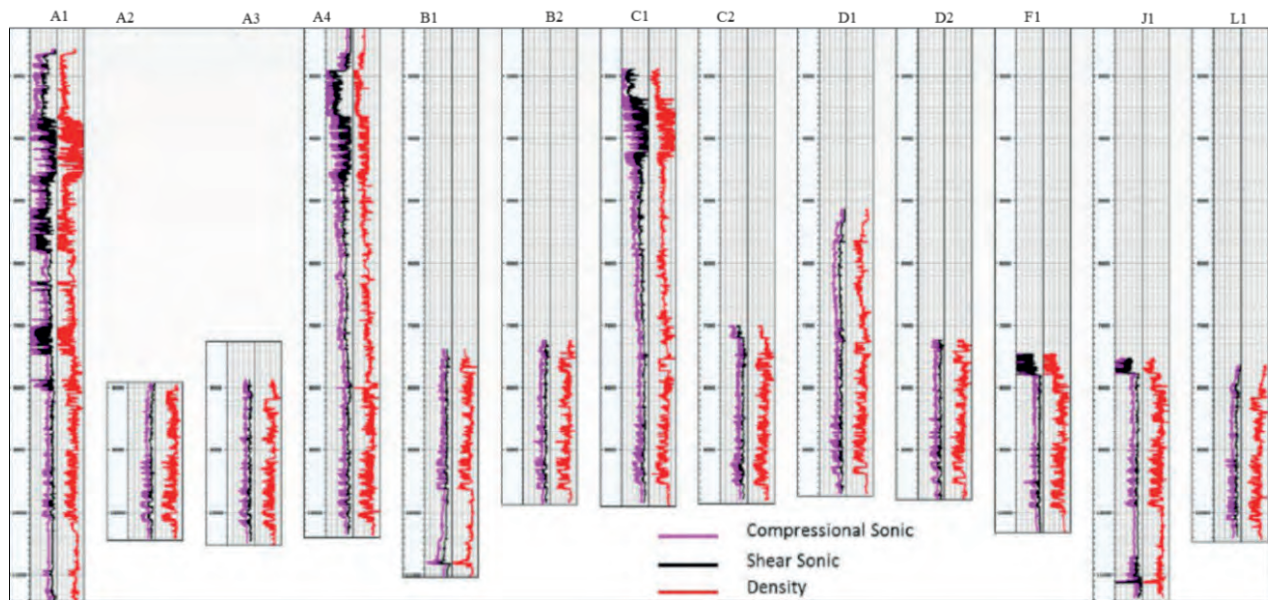


Fig. 4. Shows the measured and edited compressional and share sonic slowness and density in terms of log view.

density is also generated using calibrated Gardner type relations starting from published relations sand and shale. Once all the measured data are edited, shear velocity need to be predicted where missing on the nine wells (Kumar *et al*, 2014). Two methods are tested in parallel:

Calibrated linear relation Greenberg-Castanga (GC) type and Neural Network (NN) with inputs like compressional velocity, gamma ray and deep resistivity. Figures 5 and 6 show the histograms of the difference between measured and synthetic shear and compressional velocities. The neural network is slightly more centered and symmetrical. Therefore; this method is the preferred choice.

The Result of the Audit and Editing: Fig. 7 shows the result and QC of the edited logs for the well A1-47-02 as an example. After editing the whole gaps are filled and the abnormal values replaced. Figures 3, 4 show compressional, shear sonic and density of the thirteen wells respectively before and after editing, all the gaps are filled and the missing data have been generated where the data set are more homogeneous.

It can be observed from, the cross plots of compressional, shear sonic and density color-coded by wells volume of clay (Fig. 8), a graduation from sand to shale in sonic: shale tends to have higher shear sonic and lower compressional sonic than sand. A sort of separation can also be seen on density versus compressional sonic plot: shale tends to have higher density and may be slightly lower compressional sonic than sand.

ROCK MECHANICS LABORATORY TEST AND 1D MECHANICAL EARTH MODELS

Sample Collection and Testing

During this study, the decision was made to analyze core samples from two representative wells. Based on the availability and conditions of the cores, selective intervals were preferred. For this test we provided 22 vertically oriented, sandstone samples, and nine (9) chunks from wells A4-047-02 & D1-047-02 (Table 1). The plugs were prepared by Libyan Petroleum Institute and provided to Schlumberger Reservoir Labs, in Salt Lake City to perform the optimum analysis. The testing program consists of:

- Unconfined compression testing on odorless mineral spirits (OMS) topped-off vertical sandstone samples at room temperature to determine peak compressive strength.
- Triaxial compression testing performed at room temperature with concurrent ultrasonic velocity measurements on OMS topped-off vertical sandstone samples and.
- Petrographic analysis including laser particle size analysis (LPSA) and sieve analysis.

The purpose of testing was

- 1) To provide strength information for developing a failure locus for the material. With adequate measurements of strength on core samples, and with the availability of supplementary information such as clay content and porosity, logging-based predictions of strength may be possible.

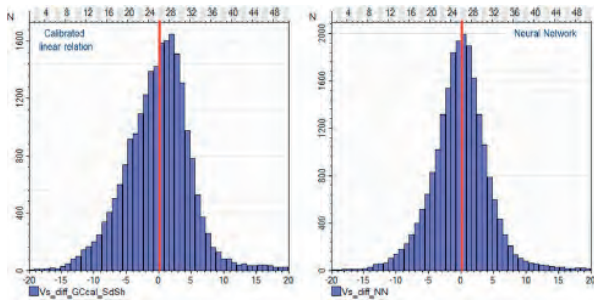


Fig. 5. Shear velocity prediction - histograms of difference between measured log and synthetics.

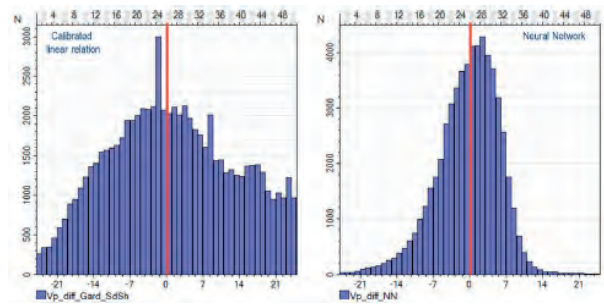


Fig. 6. Compressional velocity prediction - histograms of difference between measured log and synthetics.

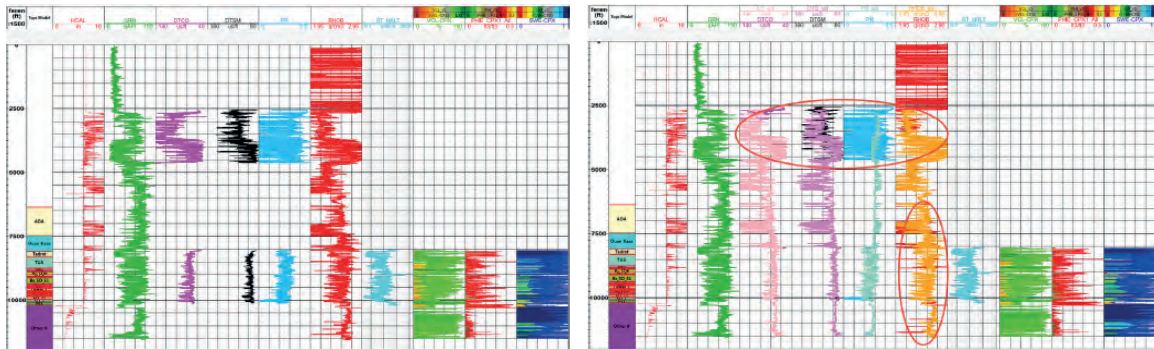


Fig. 7. QC of editing log view, measured data (left) and edited (right)- Well A1-47-02. Circles points out to slightly abnormal reading.

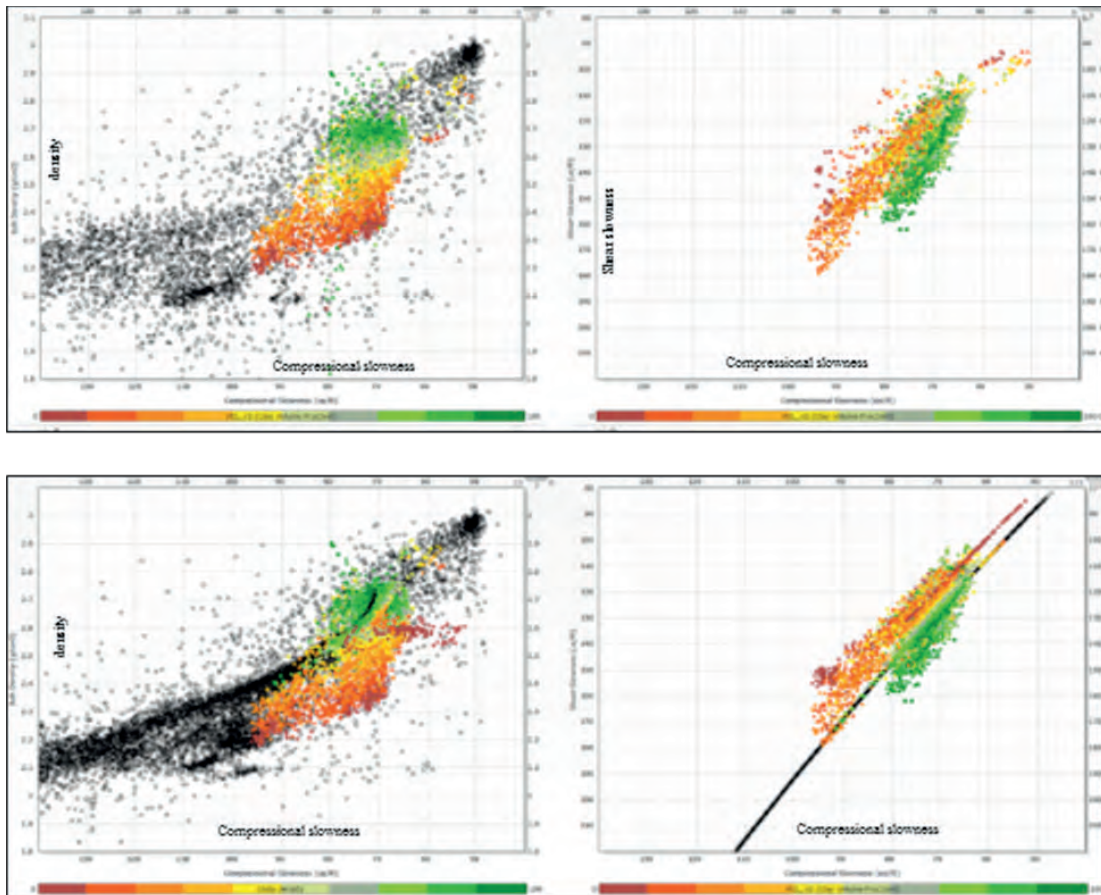


Fig. 8. Cross plot shows the QC of density vs. compressional and shear sonic vs. compressional color-coded by wells volume of clay. Measured (top), Edited (Bottom).

Table 1. Shows the sample material and testing.

Well/ Sample ID	Depth (ft)	Approx. Length in	Approx. Diameter in	Scheduled Test 1
A4-047-02				
A4 1-1	9995	2.0	1.0	UCS
A4 1-2	9995	1.8	1.0	TXC w/UVs
A4 1-3	9995	2.0	1.0	TXC w/UVs
A4 1-4	9995	2.0	1.0	TXC w/UVs
A4 2-1	10,022	2.0	1.0	UCS
A4 2-2	10,022	2.0	1.0	TXC w/UVs
A4 2-3	10,022	1.9	1.0	TXC w/UVs
A4 2-4	10,022	2.0	1.0	TXC w/UVs
D1-047-02				
D1 1-1	9006	1.9	1.0	
D1 1-2	9006	1.9	1.0	UCS
D1 2-1	9015	2.0	1.0	TXC w/UVs
D1 2-2	9015	2.0	1.0	TXC w/UVs
D1 2-3	9015	2.0	1.0	TXC w/UVs
D1 3-1	9021	1.7	1.0	UCS
D1 4-1	9027	2.0	1.0	TXC w/UVs
D1 4-2	9027	1.9	1.0	TXC w/UVs
D1 4-3	9027	2.0	1.0	TXC w/UVs
D1 5-1	9033	2.0	1.0	MTXC w/UVs
D1 5-2	9033	2.0	1.0	UCS
D1 6-1	9039	2.0	1.0	Spare
D1 6-2	9039	2.0	1.0	TXC w/UVs
D1 6-3	9039	2.0	1.0	TXC w/UVs
A4-047-02				
A4-1	9995	Chunk – 185 grams	LPSA & Sieve	
A4-2	10,022	Chunk – 197 grams	LPSA & Sieve	
A4-3	10,036	Chunk – 192 grams	Spare	
D1-047-02				
D1-1	9006	Chunk – 189 grams	LPSA & Sieve	
D1-2	9015	Chunk – 199 grams	LPSA & Sieve	
D1-3	9021	Chunk – 183 grams	Spare	
D1-4	9027	Chunk – 199 grams	LPSA & Sieve	
D1-5	9033	Chunk – 196 grams	Spare	
D1-6	9039	Chunk – 199 grams	LPSA & Sieve	

- 2) To provide static and dynamic mechanical properties information for correlating well-log data. Physical/mechanical response of a material is dependent on the rate at which it is loaded and the applied stress/strain amplitude. Logging-based measurements are in the kilohertz range; whereas, actual physical loading rates acting on a wellbore are generally much slower (pseudo-static). Even hydraulic fracturing (particularly the change in width) is a pseudo-static process. This is the rationale for performing laboratory pseudo-static testing for measurement of Young's modulus (E) and Poisson's ratio (ν), and simultaneously measuring dynamic (high loading rate and low loading magnitude) responses of core samples. This provides information for well-log calibration, to provide realistic deformation parameters (E, ν) for engineering purposes (John *et al*, 2007).
- 3) Minimize the amount of uncertainty existing in rock strength and grain size distribution, in order to improve the reliability of the Sand Prediction Model in development and to determine grain size and distribution. Based on log derived mechanical properties in situ horizontal and vertical stresses have been estimated at the depth of the samples (Table 2). This estimation has been further calibrated using core test results. Single-stage triaxial compression tests (TXC) with concurrent ultrasonic velocity measurements were performed on suites of vertical samples

at varying confining pressures (either 0.5x, 1.0x, or 1.5x the mean effective in-situ stress conditions). Additionally, when material was limited, multi-stage triaxial compression tests (MTXC) were performed on vertical samples at confining pressures equal to 1.0x and 1.5x. From stresses and strains measured during triaxial compression tests, elastic properties and compressive strength were determined for each test specimen. Static values for Young's modulus and Poisson's ratio were calculated using the following equations:

$$E_s = \delta \sigma_l / \delta \epsilon_a$$

$$\nu_s = \delta \epsilon_r / \delta \epsilon_a$$

Where:

E_s , Young's modulus,
 σ_l , axial stress,
 ν_s , Poisson's ratio, and
 $\delta \epsilon_a$, $\delta \epsilon_r$ axial and radial strains.

Static Young's modulus and Poisson's ratio correspond to the initial slope of the laboratory tests curves Axial stress vs Axial strain and Radial strain vs. Axial strain, respectively. Results of unconfined and triaxial compression tests are presented in Tables 3 and 4. Dynamic mechanical properties using ultrasonic wave transmission (with 1MHz P- and S-wave transducer) were determined concurrently during all triaxial compressional tests. Comparison of static and dynamic values of Poisson's and Young's modulus with increasing confining pressure for vertical samples are shown in Tables 5 and 6. These results allowed establishing the correlation and the corresponding correction to apply in order to drive static Young's modulus.

1D MECHANICAL EARTH MODELS (MEM)

Once the mechanical properties and stresses are derived from the wireline logging data and calibrated against the available measurements of core tests, the geomechanical evaluation process is accomplished by means of well bore stability (WBS, Biniti *et al*, 2015). The drilling integrity analysis is performed, and the results are ready to be used for the sanding analysis.

Mechanical Properties (elastic and stress)

The rock mechanical properties include the poroelastic properties (Young's modulus E; Poisson's ratio PR), Biot's coefficient (ALPHA)

Table 2. In-Situ stress conditions inferred from preliminary Mechanical Earth Models (MEM). Mean effective stress is defined as $(1/3*(\text{SigH}+\text{SigH}+\text{SigV})-\text{Pp})$. Biot’s coefficient (ALFA) assumed equal to 1.

Well ID/ Depth ft	SigH psi	SigH psi	SigV psi	PP psi	Effective Stresses: alpha = 1.0			Confining Pressure Stages (Mean-Eff-Stress)		
					Vertical psi	Horizontal psi	Mean psi	0.5x in-situ	1.0x in-situ	1.5x in-situ
A4-047-02										
9995	6102	6257	10,598	3998	6600	2182	3654	1827	3654	5482
10,022	6613	6770	10,625	4009	6616	2683	3994	1997	3994	5991
D1-047-02										
9006	6886	7430	9744	3602	6142	3556	4418	2209	4418	6627
9015	5754	5831	9754	3606	6148	2187	3507	1754	3507	5261
9021	6015	6127	9761	3608	6153	2463	3693	1847	3693	5540
9027	6381	6465	9767	3611	6156	2812	3927	1963	3927	5890
9033	6292	6399	9773	3613	6160	2733	3875	1938	3875	5813
9039	5985	6242	9780	3616	6164	2498	3720	1860	3720	5580

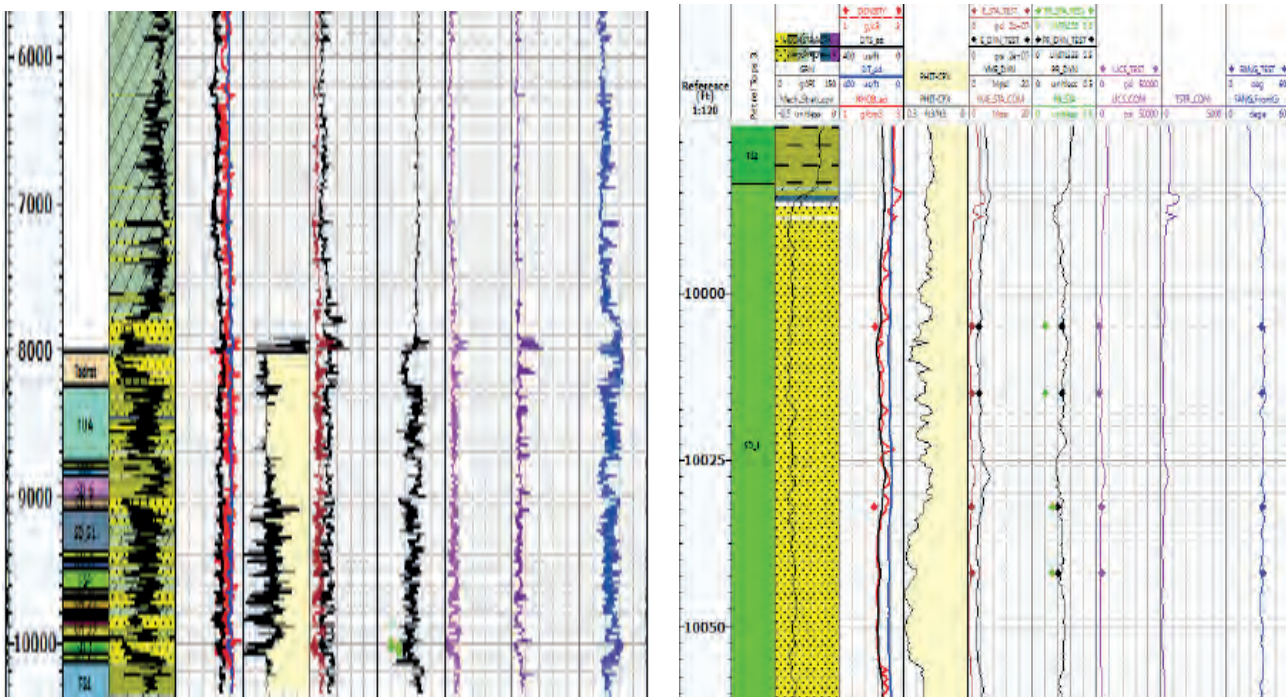


Fig. 9. a) Mechanical properties of well A4. b) Mechanical Properties of well A4.

and rock strength properties (unconfining compressional strength UCS), internal friction angle (FANG) and the tensile strength (TSTR, Gang *et al*, 2011). Log data, notably compressional and shear slowness and rock bulk density, were used to compute dynamic elastic module. Elastic properties computed from the logs are termed dynamic because the sonic measurements are conducted at high frequencies. wellbore deformation or failure is a relatively slow process compared to high frequency wave propagation. The properties computed from core tests considered to be static measurements. Static Young’s Modulus correlation has been used to calculate UCS which is the load per unit area at

which a cylindrical sample fails in compression without applying confining (cell) pressure.

To check the validity of the mechanical properties estimated in the 1D MEMs and allow a possible calibration, the lab test results of wells A4 has been plotted against in situ stress conditions Fig. 9a and b. A very good match for dynamic and static Young’s modulus was observed and no further calibration was required. However; Dynamic Poisson’s ration and static one do not seem to have a clear correlation. Consequently, static has been considered equal to dynamic one. High dispersion of experimental data is well known in the literature. It is generally observed that there is no meaningful correlation

between the values of static Poisson's ratio and other mechanical properties or physical property of the rock, expect porosity. High Poisson's ration corresponds to high porosity. UCS has been calibrated (i.e. decreased) to match with the Lab results. TSTR has been assumed equal to 10% of the UCS in the lack of specific laboratory tests. FANG results show good match and no further calibration was required.

Pore Pressure and Overburden Stress

The weight of the overburden sediments compacts the grains and squeezes the water out. The water escapes based on the permeability and rate of burial. In the study area, no evidence of overpressure is recorded in any of the 13 wells in the end of well report (EOWR). This is confirmed by measurements in MDT results. The average gradient of 0.4 psi/ft has been measured. Pore pressure (PP) profile for each well is studied. Only pore pressure of well D1 is shown in (Fig. 10).

The overburden weight per unit area is called overburden or vertical stress. Overburden stress at any given depth is the pressure exerted by the weight of the overlying sediments and can be calculated integrating the density of the overlying sediments (synthetic and measured).

Horizontal Stress

Minimum and maximum horizontal stresses are fundamental input to wellbore stability, they are used to compute failure. Horizontal stresses have been computed considering poroelastic theory involves Young's modulus, Poisson's ratio, Biot's constant (ALPHA) assumed =1, vertical stress, pore pressure.

Minimum horizontal stress also called (closure pressure) can be constrained by leak off test. In the study area, only formation integrity test (FIT) was provided therefore cannot be calibrated. and must be better corroborated by direct measurements from the upcoming drilled wells.

Maximum horizontal stress gradient is somewhat complicated as there isn't a direct measurement that could be used to infer its values. They are generally derived from the MEM and well bore stability (WBS). The result of the stress modeling of each well is studied. Fig. 11 presents the model of well A2 and A4.

Wellbore Stability (WBS) Analysis

The principal stresses around the borehole are used to determine if the borehole wall has failed or not. WBS is caused by two major types of failure, shear or tensile. Shear failure is usually caused by low mud weight; tensile failure is caused by high

Table 3. Summary of Unconfined and Triaxial Compressional Tests of well A4.

Well /sample ID	Depth ft	Bulk Density g/cm3	Confining Pressure psi	Peak Effective compressive strength psi	Effective Residual compressive strength psi	Young's Modulus	Average Poisson Ratio
A4-047-02							
A4 1-1	9995	2.160	0	1985	-	288,100	0.27
A4 1-2	9995	2.079	1827	11,908	8389	918,700	0.11
A4 1-4	9995	2.084	3654	17,357	13,973	1,295,000	0.10
A4 1-3	9995	2.156	5482	21,072	19,306	1,526,000	0.14
A4 2-1	10,022	2.120	0	3862	-	436,200	0.18
A4 2-4	10,022	2.069	1997	14,013	10,583	926,200	0.17
A4 2-3	10,022	2.091	3994	21,539	15,678	1,208,000	0.16
A4 2-2	10,022	2.096	5991	25,076	22,046	1,429,000	0.16

Table 4. Summary of Unconfined and Triaxial Compressional Tests of well D1.

Well /sample ID	Depth ft	Bulk Density g/cm3	Confining pressure psi	Peak Effective compressive strength psi	Effective Residual compressive strength psi	Young's Modulus	Average Poisson Ratio
D1-047-02							
D1 1-2	9006	2.117	0	1040	-	135,000	0.26
D1 1-1	9006	2.122	4418	16,590 (Y)	-	1,182,000	0.10
(Multi-Stage-TXC)			6627	21,606	N.A.	1,618,000	0.18
D1 2-2	9015	1.894	1754	9129	7812	756,400	0.12
D1 2-1	9015	1.922	3507	15,333	14,034	1,093,000	0.14
D1 2-3	9015	1.909	5261	18,364	16,526	1,209,000	0.14
D1 3-1	9021	2.206	0	5922	-	1,198,000	0.33
D1 4-3	9027	2.268	1963	13,326	8540	1,291,000	0.14
D1 4-1	9027	2.237	3927	20,689	14,421	1,410,000	0.20
D1 4-2	9027	2.269	5890	28,536	23,769	2,464,000	0.16
D1 5-2	9033	2.080	0	791	-	120,100	0.30
D1 5-1	9033	2.069	3875	13,716 (Y)	-	917,200	0.12
(Multi-Stage-TXC)			5813	17,072	16,863	1,412,000	0.19
D1 6-2	9039	2.048	3720	16,371	14,955	1,154,000	0.08
D1 6-3	9039	2.055	5580	20,812	18,470	1,305,000	0.10

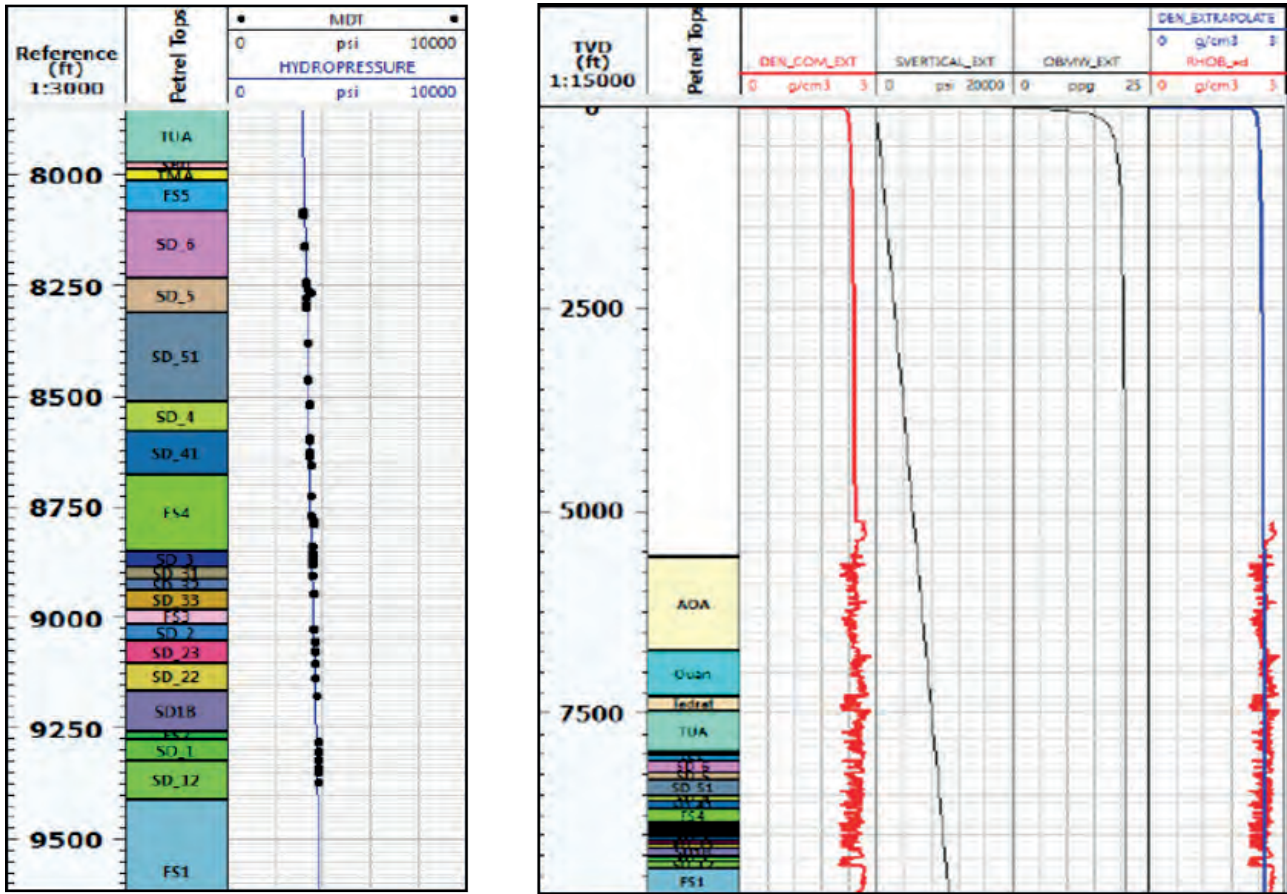


Fig. 10. Pore pressure profile in pressure (Hydropressure) against MDT measurements of well A4

Table 5. Dynamic vs. Static Mechanical properties determined during confining tests for wells A4. cells (--) shows poor S-wave data quality. Dynamic NA.

Well/ Sample ID	Depth ft	Effective confining pressure psi	Static Young's modulus psi	Dynamic Young's modulus psi	Static Poisson's Ratio (average)	Dynamic Poisson's ratio	Dynamic /static Young's Modulus	Dynamic / Static poison's Ratio
A4-047-02								
A4 1-2	9995	1827	918,700	3,022,000	0.11	0.24	3.29	2.18
A4 1-4	9995	3654	1,295,000	3,445,000	0.10	0.23	2.66	2.30
A4 1-3	9995	5482	1,526,000	3,482,000	0.14	0.24	2.28	1.71
A4 2-4	10,022	1997	926,200	--	0.17	--	--	--
A4 2-3	10,022	3994	1,208,000	--	0.16	--	--	--
A4 2-2	10,022	5991	1,429,000	--	0.16	--	--	--
Average:							2.74	2.07

Table 6. Dynamic vs. Static Mechanical properties determined during confining tests for well D1. cells (--) shows poor S-wave data quality. Dynamic NA.

Well/ Sample ID	Depth ft	Effective confining pressure psi	Static Young's modulus psi	Dynamic Young's modulus psi	Static Poisson's Ratio (average)	Dynamic Poisson's ratio	Dynamic /static Young's Modulus	Dynamic / Static poison's Ratio
D1-047-02								
D1 1-1	9006	4418	1,182,000	2,994,000	0.10	0.29	2.53	2.90
		6627	1,618,000	2,886,000	0.18	0.31	1.78	1.72
D1 2-2	9015	1754	756,400	2,488,000	0.12	0.26	3.29	2.17
D1 2-1	9015	3507	1,093,000	2,957,000	0.14	0.23	2.71	1.64
D1 2-3	9015	5261	1,209,000	2,956,000	0.14	0.23	2.44	1.64
D1 4-3	9027	1963	1,291,000	4,897,000	0.14	0.22	3.79	1.57
D1 4-1	9027	3927	1,410,000	4,822,000	0.20	0.23	3.42	1.15
D1 4-2	9027	5890	2,464,000	5,622,000	0.16	0.20	2.28	1.25
D1 5-1	9033	3875	917,200	3,201,000	0.12	0.25	3.49	2.08
		5813	1,412,000	3,060,000	0.19	0.24	2.17	1.26
D1 6-2	9039	3720	1,154,000	----	0.08	--	--	--
D1 6-3	9039	5580	1,305,000	0.10	--	--	--	--
Average:							2.79	1.74

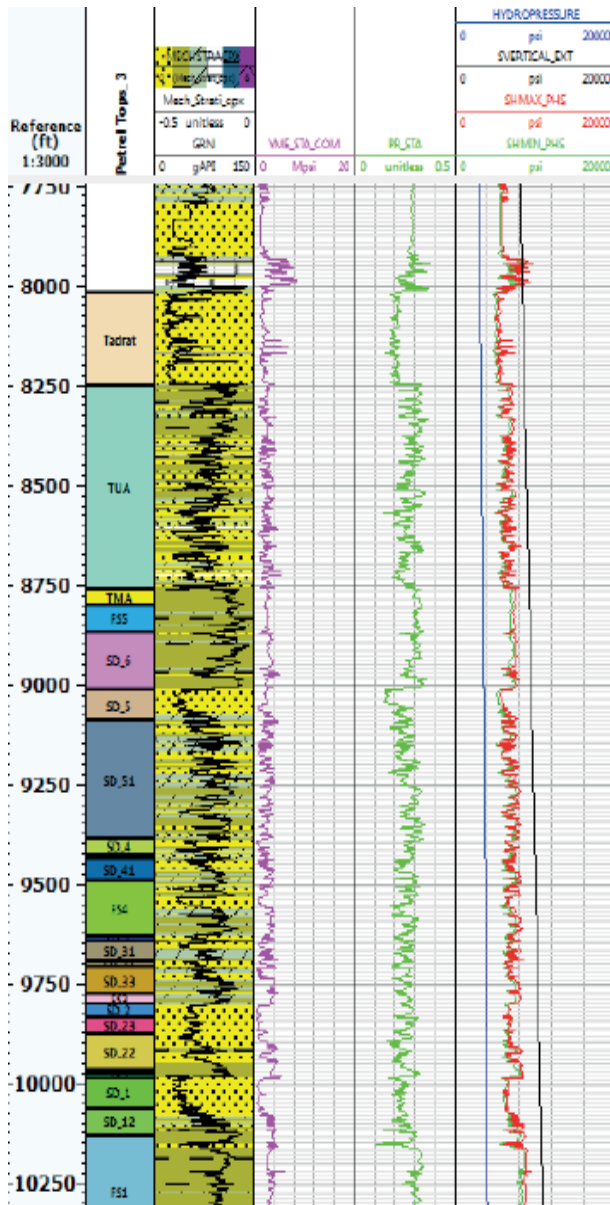


Fig. 11. Stress modeling results of well A2 (left) and well A4 (right). YME_sta_com= static young's modulus; PR_sta= static Poisson's ratio, Hydopressure= pore pressure; SHmax_phs= maximum horizontal stress, SHMIN_phs= minimum horizontal stress.

mud weight (Assif and Ni (2018). Mud weight is the output of the WBS. There are four limits defining the mud weight window. Pore pressure, breakout, mud loss and breakdown.

The result of WBS analysis for the studied well A1 shows a good match between predicted wellbore instability, calipers and drilling experimental events.

Predicted damage is also in good agreement with borehole images. FMI indicates that because of uncontrollable mud weight this well was highly affected by borehole breakout and drilling induced fractures. Most wells predicted damage reproduces

satisfactory indication from calipers admitting a manageable damage of 10%.

SAND PRODUCTION ANALYSIS

Sand production analysis performed using schlumberger software Sand Management Adviser (SMA). The sand prediction model can also be used to assess changes of the critical drawdown pressure (CDD) for an open hole or perforated cased hole that may occur over the life of a field undergoing a depletion.

Fig. 12 illustrates a typical plot of single-depth sanding analysis and the definition of CDD pressure. The difference between the reservoir pressure and the bottom hole flowing pressure defines the drawdown. The boundary line between the red zone and the green zone defines the critical drawdown at different reservoir pressures. The reservoir pressure at which the boundary line crosses the diagonal is the critical reservoir pressure for sand-free production.

The CDD pressure decreases whilst the reservoir depletes and disappears at the critical reservoir pressure. The well cannot produce in the zone above the diagonal because the bottom hole flowing pressure (BHFP) is higher than the reservoir pressure in that zone. If the operation conditions lie in the green zone, the well can produce sand free. On the other hand, sand will be produced if the operating conditions lie in the red zone.

Clearly, the CDDP decreases with reservoir depletion which means the possibility for sanding to occur increases. The analysis and results allow comparison of sanding risk for different completion strategies at different stages in the life of the field. The analysis can identify high risk zones in the completion interval. These intervals should be considered for isolation because they may be expected to fail further under different production conditions.

Some of the analyzed offset seven out of thirteen wells have exhibited sand production phenomenon during Drill Stem Tests (DST). In this study, the proposal is to calibrate the sanding prediction on the produced tests to be able to apply the model to predict sand in the planned wells (Assif and Ni, 2018). An example of these results is shown in (Fig. 13). Well A1 where clearly the estimated CDD at pre-production conditions (CDDP-0) is almost the same for the three-perforation azimuth phased every 60 degrees (at 0° N, 60° N and 120°N). Figure 13 also indicates that four out of five DST,

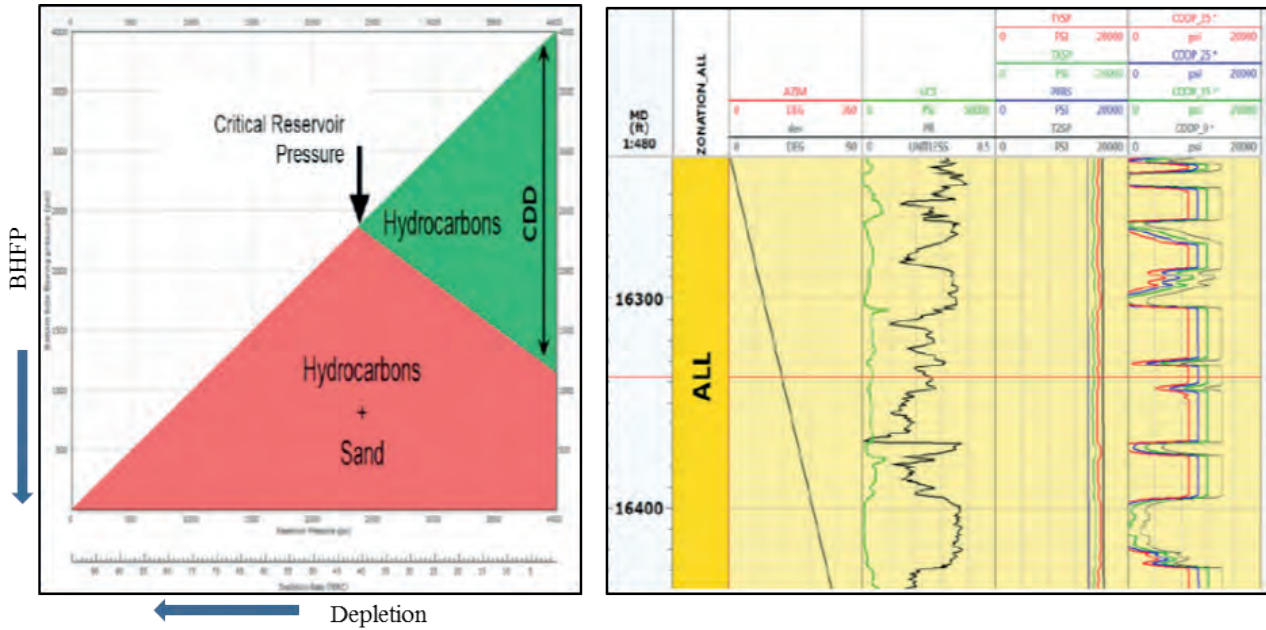


Fig. 12. Typical plot for sand prediction for single depth analysis (left) for an interval analysis (right), CDDP are calculated for different reservoir states corresponding in this case to 0%, 15%, 25% and 35% of deletion.

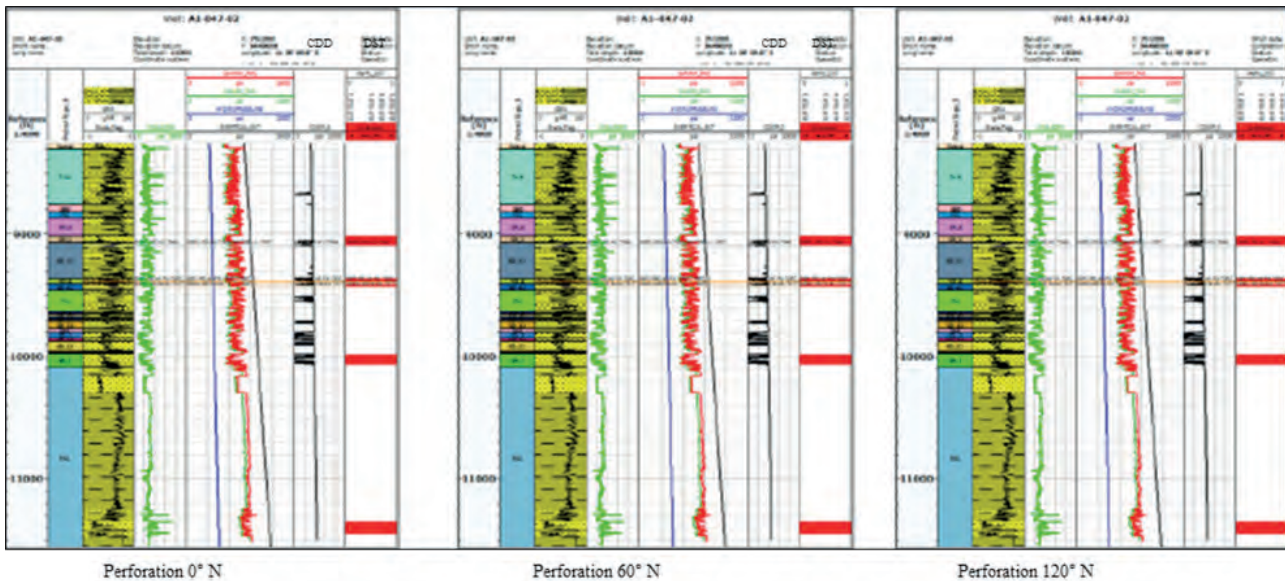


Fig. 13. Critical drawdown pressures computed for different perforation tunnel azimuth. DST perforation intervals (red last track) show sand production in agreement with the computed CDD.

the model predicted sand production. Results of the other wells with respect to sanding are in a good agreement with the computed critical drawdown. Well B2 for instance, doesn't appear in the list of the wells where sanding was produced during DSTs. However, computed CDDP predicted some sanding at the depth of the perforation (Zahirin *et al*, 2010).

CONCLUSIONS

Geomechanical studies of the available thirteen wells have been performed. The mechanical earth

model and wellbore stability analysis performed to assess mechanical properties and stresses that have been used for sanding analysis. A preliminary petrophysical and rock physics analysis of log data from these wells allowed to calculate synthetic logs where data are missing. The main results are:

Phase 1: Data Audit & Rock Physics

Good logging coverage: Density, GR, CAL, VCL, PHIE, SW available for all wells, P-Sonic available for 11 wells, S-Sonic for 4 wells. Editing performed to fill gaps and correct bad obvious

reading. Synthetic curves generated using Neural Network technique. For the overburden, synthetic density logs have been generated.

Phase 2: 1D Mechanical Earth Models and Wellbore Stability Analyses

Different correlations have been used to calculate the mechanical properties (elastic and strength). Used correlation from the dynamic to static Young's modulus well fits laboratory tests results. Correction from the dynamic to static Poisson's ratio in sands not applied given the high dispersion and low correlation of experimental data Calibration of strength properties (UCS, FANG) in sands has been performed based on tests results.

Wellbore stability models are in agreement with reported drilling events. It is observed that some manageable wellbore damage has been generated during drilling, damage can be quantified at about 10% (Depth of Damage).

Wells stress models are calibrated on wellbore stability analyses. Direct measurements of the least principal stress at casing point leak off test (LOT, ELOT) were not available in any of the 13 wells. Only formation integrity tests (FIT) were performed. To improve the reliability of the least principal stress (minimum horizontal stress) estimation and reduce uncertainty appropriate stress measurements are necessary.

Phase 3: Sanding Analysis

Laboratory tests results rank Lower Acacus sands from very weak to weak. Grain size is a fundamental input parameter in sanding analysis. In order to include Grain Size variability along the analyzed sections Neural Networks method has nine (9) sanding analyses have been performed, all analyses confirm occurrence of sanding in some critical sections at actual reservoir pressure.

Predicted sanding on existing wells is in a good agreement with observation from DST.

No influence of perforation orientation is observed due to a very limited stress anisotropy inferred from the stress model calibrated on wellbore stability analyses. Sanding is mainly controlled by UCS.

REFERENCES

- Assef, M. H. and Ni, Q. (2018). Numerical Modeling of Onset and Rate of Sand Production in Perforated Wells. *Jour. Petr. Explor. Prod. Tech.*, **8** (4): <https://doi.org/10.1007/s13202-018-0443-6>.
- Binti, A. I. A.; Brandt, I.; Gunasekera, D.; Hatveit, B.; Havre, K.; G. Weisz and Xu., Z. G. (2015) Multiphase Flow Simulation Optimizing Field Productivity. https://www.slb.com/~media/Files/resources/oilfield_review/ors15/spr15/03-multiphase-flow. *The Oil field Review*, (1): 26–37.
- Case Study-Brazil (2013). Petrobras Enhances Reservoir Performance With Geomechanics Evaluation in Water Injection Operation. http://www.slb.com/resources/case_studies/dcs/reservoir_consulting/geomechanics_offshore_brazil_cs.aspx.
- Gang, H.; Shepstone, K.; Harmawan, I.; Jusoh, U. H.; Sue Lin, L. and Pringle, D. (2011). A Comprehensive Study of Sanding Rate from A Gas Field: from Reservoir to Completion, Production, and Surface Facilities. *SPE Journal*, **16** (2): 463–81. <https://doi.org/10.2118/123478-PA>, 2011
- John, C.; Frederiksen, R. A.; Hasbo, K.; Green, S.; Judzis, A.; Martin, J. W. and Suarez-Rivera, R. (2007). Rocks Matter: Ground Truth in Geomechanics. https://www.slb.com/~media/Files/resources/oilfield_review/ors07/aut07/rocks_matter.pdf *Oilfield Review* **19** (3): 36–55., 2007
- Kumar, S. S.; De Groot, L. and Graven, H. (2014). An Innovative Approach for Sand Management with Downhole Validation. *Soc. Petr. Eng.*, **15** (2): <https://doi.org/10.2118/168178-MS>.
- Zahirin, R. M.; Frydman, M.; Sepulveda, W.; Garcia, G.; Benavides, M. and Matulevich A. (2010). Integrated Approach: Perforation System Optimization for Sand Prevention. *Soc. Petr. Eng.*, **14** (1): <https://doi.org/10.2118/128569-MS>.